Published in final edited form as:
Vaccine. 2010 December 6; 28(52): 8315–8326. doi:10.1016/j.vaccine.2010.07.070.

High-throughput automated image analysis of neuroinflammation and neurodegeneration enables quantitative assessment of virus neurovirulence

Olga A. Maximova[*], **Brian R. Murphy**[1], and **Alexander G. Pletnev**[**]
Laboratory of Infectious Diseases, NIAID, NIH, Bethesda, MD 20892, United States

Olga A. Maximova: maximovao@niaid.nih.gov; Brian R. Murphy: bmurphy@niaid.nih.gov; Alexander G. Pletnev: apletnev@niaid.nih.gov

Abstract

Historically, the safety of live attenuated vaccine candidates against neurotropic viruses was assessed by semi-quantitative analysis of virus-induced histopathology in the central nervous system of monkeys. We have developed a high-throughput automated image analysis (AIA) for the quantitative assessment of virus-induced neuroinflammation and neurodegeneration. Evaluation of the results generated by AIA showed that quantitative estimates of lymphocytic infiltration, microglial activation, and neurodegeneration strongly and significantly correlated with results of traditional histopathological scoring. In addition, we show that AIA is a targeted, objective, accurate, and time-efficient approach that provides reliable differentiation of virus neurovirulence. As such, it may become a useful tool in establishing consistent analytical standards across research and development laboratories and regulatory agencies, and may improve the safety evaluation of live virus vaccines. The implementation of this high-throughput AIA will markedly advance many fields of research including virology, neuroinflammation, neuroscience, and vaccinology.

Keywords

Virus neurovirulence; Nonhuman primates; Neuroinflammation; Neurodegeneration; Digital pathology; Automated image analysis (AIA)

Live virus vaccines against viral encephalitides, as well as against certain virus infections with neurovirulent potential, must be effective and safe with particular focus on the CNS. Historically, the safety of such live vaccines, beginning with vaccines against poliomyelitis and yellow fever, was assessed by evaluation of virus neurovirulence in intracerebrally inoculated monkeys. Although controversial in some instances [1–6], neurovirulence testing in monkeys remains the only accepted method to assess the CNS safety of live virus vaccines against neurotropic viruses prior to their evaluation and use in humans.

Analysis of CNS histopathology induced by neurotropic viruses or vaccine candidates, i.e., their neurovirulence, is traditionally performed by using semi-quantitative scoring

[*]Corresponding author. Tel.: +1 301 443 5953; fax: +1 301 480 4509. [**]Co-corresponding author. Tel.: +1 301 402 7754; fax: +1 301 480 4509.
[1]Tel.: +1 301 594 1616; fax: +1 301 480 5053.

Contributors: OAM, BRM, and AGP conceived and designed the experiments and analyses. OAM and AGP performed the experiments and acquired the data. OAM, BRM, and AGP analyzed the data, wrote, and critically revised the paper.

Conflict of interest statement: The authors do not have a conflict of financial or other interest.

techniques (i.e., categorical/arbitrary/subjective grading scales) to evaluate the histopathological changes in routinely stained (H&E and/or Nissl) sections of selected "indicator centers" [7,8], which represent the most frequently affected CNS regions. The histopathological features generally assessed by this semi-quantitative scoring usually include inflammatory infiltrates (perivascular and parenchymal), microglial nodules, and neuronal changes, that are common for a majority of viral encephalitides. Although the semi-quantitative histopathological grading was useful for evaluation of neurovirulence of a variety of viruses [4,7–21], this method is inherently subjective and potentially biased. In the current era of molecular and digital pathology, it seems prudent to explore the use of a more accurate quantitative method for evaluation of biological markers of neuroinflammation and neurodegeneration to assess virus-induced neuropathology and neurovirulence with increased objectivity.

The intracerebral inoculation of monkeys with attenuated flaviviruses results in microglial activation, infiltration by peripheral immune cells, and neurodegeneration [19,22]. Accordingly, we used a modified histopathological scoring system to separately evaluate cellular inflammatory infiltration (CII), microglial activation (MGA), and neuronal degeneration (ND) [19]. Based on this approach, we were able to demonstrate differences in magnitude and spatiotemporal patterns of neuroinflammation induced by antigenically divergent attenuated flaviviruses. Using immunohistochemical analysis, we showed that inflammatory foci in the virus-infected CNS are composed of $CD68^+$ macrophages/microglia, $CD3^+$, $CD4^+$, and $CD8^+$ T cells, and $CD20^+$ B cells [19,22].

In the current study, we have expanded the range of cellular markers and analyzed the extent of neurodegeneration in virus-infected CNS by measuring the immunoreactivity for the specific neuronal marker NeuN. We demonstrate that the decreased immunoreactivity for the NeuN reliably reflects both neurodegeneration and neuronal loss. The new data were considered together with histopathological scores and immunoreactivity data for inflammatory cellular markers obtained previously for monkeys infected with Langat virus (LGTV), a chimeric tick-borne encephalitis TBEV/DEN4Δ30 virus, or the yellow fever 17D (YF 17D) vaccine virus [19,22]. Of these three flaviviruses, only the YF 17D virus exhibits a low level of neurovirulence and is safe for human vaccinees. The Langat and TBEV/DEN4Δ30 viruses are more neurovirulent and are not acceptable for human vaccination against tick-borne encephalitis [19]. To determine whether the quantitative image analysis of neuroinflammation and neurodegeneration can be used to accurately assess the level of virus neurovirulence, we compared this analysis with semi-quantitative data generated by conventional histopathological scoring. We show that the magnitude of neuropathology measured by the amount of immunoreactivity for cellular markers of lymphocytic infiltration, microglial activation, and neurodegeneration correlated strongly and significantly with relevant histopathological scores demonstrating that the AIA of virus-induced neuroinflammation and neurodegeneration is useful for evaluation of virus neurovirulence.

1. Materials and methods

1.1. Viruses

LGTV wild-type strain TP21 was received from the Rockefeller Foundation Collection and amplified in Vero cells [31]. The chimeric recombinant TBEV/DEN4Δ30 virus, containing the prM and E genes of the TBEV strain Sofjin and a 30-nucleotide deletion in the 3′ non-coding region of the genome, was originally recovered after transfection of Vero cells with RNA transcripts of its full-length chimeric cDNA genome [32]. The YF 17D vaccine virus was received from Sanofi Pasteur, Inc. (Swiftwater, PA) and amplified by one passage in Vero cells [19].

1.2. CNS tissue

The CNS tissue sections used for this study were from rhesus monkeys (*Macaca mulatta*) intracerebrally inoculated with 10^5 plaque-forming units of TBEV/DEN4Δ30 (n = 3), LGTV (n = 4), YF 17D (n = 4), or mock-inoculated (n = 1) with Leibovitz's L-15 medium (Invitrogen; Carlsbad, CA). All animals used for this study were euthanized on 21 day post-inoculation. The clinical, virological, histopathological, and immunohistochemical data for these animals were described previously [19,22]. In this study, we analyzed the following CNS Regions of Interest (ROIs): basal ganglia (caudate nucleus, putamen, and globus pallidus), thalamus, and spinal cord (cervical and lumbar regions). These CNS ROIs were chosen since they provided well-defined anatomical boundaries for quantitative analysis and were among structures consistently affected by flaviviruses and designated as "indicator centers" [8]. The series of 5 μm tissue sections were routinely processed for hematoxylin and eosin (H&E) or Nissl (Cresyl violet) staining (not shown), or were immunostained for specific cellular markers.

1.3. Semi-quantitative histopathological evaluation

To evaluate the neurovirulence of attenuated flaviviruses we previously determined the histopathological scores in the CNS of intracerebrally inoculated rhesus monkeys using semi-quantitative analysis [19]. The scores (0, no lesions; 1, minimal; 2, mild; 3, moderate; 4, severe) were assigned separately to (i) cellular inflammatory infiltration (CII) and (ii) microglial activation and neuronal degeneration (MGA/ND). In this study, we used those previously generated scores for comparison and validation of the results of the AIA of neuroinflammation and neurodegeneration. The grading scale incorporating only CNS ROIs analyzed in this study can be found in Supplementary Table 1.

1.4. Immunohistochemistry

Cell phenotyping was performed using antibodies (Biocare Medical; Concord, CA) to human CD3 (pan-T cell marker), CD20 (pan-B cell marker), and antibody to CD68 (Dako; Carpinteria, CA) (directed against a lysosomal protein expressed by phagocytic macrophages of microglial and monocytic origin), and NeuN (Millipore; Billerica, MA) (neuronal marker). Further processing for diaminobenzidine colorimetric detection and use of controls were as described previously [19]. Dako Autostainer System (Dako; Carpinteria, CA) was used for immunostaining on each batch of slides automatically to minimize variability between sections.

1.5. Digital pathology

Whole-tissue sections containing entire CNS ROIs were mounted on slides, stained with H&E or immunostained for cellular markers, and were digitalized in batches at a 20× magnification using ScanScope T2 (Aperio, Vista, CA). Spectrum software (Aperio, Vista, CA) was used for the data management and Aperio ImageScope software (Aperio, Vista, CA) was used for a whole-tissue section image viewing and analysis. Primate Brain Maps: Structure of the Macaque Brain, CD [33] and *M. mulatta* brain maps (NIMH, NIH; http://brainmaps.org) were used for neuroanatomical orientation and mapping of the CNS ROIs.

1.6. Automated image analysis (AIA)

A detailed description of the steps employed in the image analysis of immunostained cellular markers in the primate CNS was described by us previously [22]. Briefly, a hue-saturation-intensity color threshold detection system and positive pixel count algorithm were used to quantify the amount of a specific immunostaining present within the entire digitalized area of the CNS ROI. The algorithm input parameters were selected for each

cellular marker and the algorithm was tested on a variety of digitalized CNS ROIs before its performance was evaluated as reliable and reproducible. Once established, the algorithm input parameters for each cellular marker were kept constant and the algorithm was applied to all CNS ROIs of each monkey. The digitalized area of the entire CNS ROI present in a section was viewed on the computer monitor at a low magnification using Aperio ImageScope software (Aperio, Vista, CA), outlined, and the total area was measured in mm^2. The number of positive pixels (image resolution: 0.5 μm per pixel) was determined within the entire CNS ROI using a specific immunostaining algorithm. The immunoreactivity (IR) for each cell phenotype ($CD3^+$ T cells, $CD20^+$ B cells, $CD68^+$ microglia/macrophages, or $NeuN^+$ neurons) was calculated as the number of positive pixels per mm^2 of the entire CNS ROI. The IR measured using this approach provides an overall quantitative estimate of the neuroinflammation and neurodegeneration induced by each virus under study and reflects the number of cells of each specific phenotype involved.

1.7. Statistical analysis

The correlation between the histopathological scores for CII or MGA/ND and the values of IR for specific cellular markers in the CNS ROIs of each monkey was assessed using Pearson correlation analyses (95% confidence intervals). Results from the correlation analyses are represented by *R*, the correlation coefficient, and *P*-values below 0.05 were considered significant. ANOVA analysis (alpha 0.05) with Tukey–Kramer post hoc test was used for multiple comparisons of the viruses based on the histopathological scores or based on the IR for the specific cellular marker. Significance was assumed for probability values of $P < 0.05$.

2. Results

2.1. Comparison of lymphocytic immunoreactivity and histopathological scores

Two general approaches can be used to evaluate the severity of cellular inflammatory infiltration in the CNS induced by viruses with different neurovirulence. The conventional semi-quantitative approach relies on histopathological analysis of routinely stained (H&E and/or Nissl) sections and assignment of cellular inflammatory infiltration (CII) scores based on the number of perivascular infiltrates and degree of parenchymal infiltration. The representative H&E-stained sections that contained the entire areas of the CNS Regions of Interest (CNS ROIs) including the basal ganglia (caudate nucleus, putamen, and globus pallidus), thalamus, and spinal cord (cervical and lumbar regions) were digitalized and are shown in Figs. 1a and b and 2a and b and Supplementary Fig. 1a and b. These digitalized whole-tissue sections provide an overall view of the inflammatory cell infiltration in the entire CNS ROIs of a mock-inoculated control or virus-infected monkeys. The new approach is based on automated image analysis (AIA) that measures the immunoreactivity (IR) of the infiltrating T and B cells using specific lymphocytic markers (CD3 and CD20, respectively) and provides quantitative data on the overall level of perivascular and parenchymal lymphocytic infiltration (Figs. 1c–h and 2c–h and Supplementary Fig. 1c and d).

To validate the results of the AIA of lymphocytic IR against the CII scores, we performed Pearson correlation analyses. We compared the CD3-IR, CD20-IR, or pooled CD3/CD20-IR values within the CNS ROIs with the CII scores for each of twelve monkeys (one mock-inoculated control monkey and groups of three or four monkeys infected with TBEV/DEN4Δ30, LGTV, or YF 17D virus) (Fig. 3). This analysis demonstrated that either CD3-IR or CD20-IR alone, or pooled CD3/CD20-IR (reflecting overall lymphocytic IR) correlated strongly and significantly with CII scores in all CNS ROIs (*R*, 0.719–0.953; $P < 0.01$). In addition, statistical analysis demonstrated that CD3-IR, CD20-IR, or CD3/CD20-IR values

were similar to CII scores in identifying differences between the viruses based on induced inflammatory cell infiltration (as indicated by asterisks in Fig. 3). These results show that both methods can reliably evaluate the overall inflammatory cell infiltration in the virus-infected CNS.

2.2. Comparison of microglial immunoreactivity and histopathological scores

Two different approaches can also be used to evaluate the magnitude of microglial activation in the virus-infected CNS. A conventional semi-quantitative histopathological analysis generates scores based on the number of microglial nodules and an estimation of the degree of diffuse patterns of microglial activation in the H&E and/or Nissl stained sections. This type of microscopic analysis is complicated and time-consuming since the routine histological stains are not cell type specific and assessment is largely based on the presence of focal and/or diffuse parenchymal “hypercellularity”, which is often topographically associated with degenerating/dying neurons (e.g., neuronophagia). In contrast, the AIA allows direct evaluation of microglial activation by measuring the IR for the specific microglia/macrophage marker CD68 and provides a more accurate assessment of both focal and diffuse microglial activation. The assessment of the CD68-IR in the digitalized whole-tissue sections is illustrated in Figs. 4a and c, 5a and c.

Pearson correlation analysis demonstrated that the CD68-IR values correlated strongly and significantly with histopathological scores for microglial activation/neuronal degeneration (MGA/ND Score) within all CNS ROIs (Fig. 6a–c; R, 0.795–0.877; $P \leq 0.001$). However, it should be noted that there were some discrepancies between these two evaluation approaches. First, using the AIA we measured substantial CD68-IR in the zone of virus inoculation (thalamus) and partially in the adjacent areas of basal ganglia [22]. This microglial response was largely attributed to tissue injury due to inoculation since it was observed in both mock-inoculated and virus-infected monkeys. In contrast, these injection-related lesions were considered non-specific and received a score of zero by histopathological scoring [19]. Second, CD68-IR may also reflect concomitant recruitment of peripheral macrophages in addition to activated microglia. Third, the histopathological scores included not only microglial activation but also neuronal degeneration. Taken together, the discrepancies in the two evaluation approaches could explain why MGA/ND histopathological scores were often statistically more discriminating ($P < 0.05$) for viruses with different neurovirulent phenotypes than CD68-IR values (Fig. 6a and c). Therefore, we sought to address the degree of neurodegeneration in virus-infected CNS quantitatively and independent of microglial activation.

2.3. Image analysis of neurodegeneration

To assess the degree of neurodegeneration in a quantitative manner we performed immunohistochemical analysis with the specific neuronal marker NeuN. Neurons with normal morphology demonstrated strong NeuN-IR in the nuclei, cytoplasm, and proximal processes. In contrast, degenerating neurons showed either significantly decreased NeuN-IR or were not immunoreactive (Figs. 4b and d and 5b and d and Supplementary Fig. 2a and c). Therefore, the analysis of NeuN-IR allowed for the assessment of the degree of neurodegeneration in the virus-infected CNS. We next measured the NeuN-IR in the CNS ROIs using the AIA (Fig. 5b and d and Supplementary Fig. 2b and d).

2.4. Comparison of neuronal immunoreactivity and histopathological scores

The NeuN-IR values within the CNS ROIs for each of twelve monkeys (mock-inoculated control monkey and three groups of virus-infected monkeys) were plotted against the MGA/ND scores and are shown in Fig. 6d and f. The NeuN-IR values showed very strong and significant negative correlation with MGA/ND scores in all CNS ROIs (R, −0.890 to

−0.946; $P < 0.001$). In other words, in the virus-infected CNS, NeuN-IR decreased with increased MGA/ND scores. In addition, NeuN-IR values were similar to MGA/ND scores in discriminating the viruses based on the degree of the induced neurodegeneration ($P < 0.05$) (Fig. 6d and f).

2.5. Relationship between microglial and neuronal immunoreactivity

Not surprisingly, in the CNS of virus-infected monkeys, the neurodegeneration assessed by NeuN-IR demonstrated strong and significant negative correlation with microglial activation measured by CD68-IR (Fig. 6g–i; R, −0.736 to −0.857; $P < 0.01$). As further demonstration of this relationship, vigorous microglial activation (intense CD68-IR) was often observed at the sites of neurodegeneration (decreased or absent NeuN-IR) (Figs. 4 and 5c and d). These findings indicate that the magnitude and extent of microglial activation (CD68-IR) may serve as a reliable indirect marker of neuronal distress/degeneration in virus-infected CNS.

2.6. Discussion

In this study, we explored the potential of a high-throughput AIA of neuroinflammation and neurodegeneration for quantitative assessment of virus neurovirulence in monkeys. Using immunohistochemistry to detect cellular markers, digitalized whole-tissue section slides, and AIA algorithms, we quantitatively evaluated major features of the virus-associated CNS histopathology including cellular inflammatory infiltration, microglial activation, and neurodegeneration. Our results provide the first comprehensive comparison of the quantitative data obtained using the AIA and conventional semi-quantitative histopathological scoring.

The histopathological basis for the majority of viral encephalitides is characterized by damage to the CNS parenchyma (neuronal cell death), focal/nodular proliferation of microglia and astroglia, neuronophagia, and focal/nodular infiltration by lymphocytes and macrophages [23,24]. The most comprehensive approach to develop a semi-quantitative histopathological grading scale for evaluation of flavivirus neurovirulence in monkeys was undertaken more than 40 years ago by Nathanson et al. [7]. This grading scale was thereafter adopted or modified to assess the neurovirulence of different viruses [4,10–21]. The published scales usually incorporate most of the histopathological features by grouping the lesions into grades based on their severity/extent and/or qualitative estimate (minimal and/or mild, moderate, severe and/or overwhelming). Some scales described in the literature are more detailed and comprehensive than others. Overall, this type of analysis is prone to subjectivity and bias and is largely influenced by a “dynamic range” of virus-induced CNS histopathology.

It should be emphasized that the original grading scales [7–10] were developed to cover the “broadest spectrum” of the CNS histopathology induced by flaviviruses with varying levels of neurovirulence (listed from least to greatest level of neurovirulence): dengue type 4, yellow fever 17D, Langat, West Nile, and Japanese encephalitis viruses. When only attenuated viruses are evaluated using a scale calibrated for the severe neuropathology induced by neurovirulent wild type viruses (usually requiring a high level of biosafety), the use of such a broad grading scale might pose a significant limitation by compressing the usable dynamic range at the lower end of such a scale. In practice, those promising vaccine candidates that demonstrated sufficient attenuation during preclinical *in vitro* testing and *in vivo* evaluation in small laboratory animals, and then “graduated” to evaluation of neurovirulence in monkeys, would not induce severe CNS histopathology of grade 4 on these scales. Indeed, numerous studies have reported that various attenuated viruses usually induced minimal or mild and rarely moderate CNS histopathology on these scales [13–17,20]. In our recent report [19] and in this study, we used an expanded grading scale that

included separate categorization of cellular inflammatory infiltration and microglial activation/neuronal degeneration and was tailored to the maximal magnitude of the observed virus-associated histopathology. This approach enabled us to better differentiate the degree of neurovirulence associated with a variety of attenuated flaviviruses. We believe that such an approach is favorable and caution against the use of broad-spectrum grading scales as they may not be sufficiently sensitive to detect subtle differences in neurovirulence between attenuated viruses and, if available, appropriate reference viruses. This concern is particularly important for the safety evaluation of live attenuated vaccines against neurotropic viruses and calls for new testing strategies or improvement of existing methodologies.

The need to develop more clearly defined criteria for assessment of virus neurovirulence and vaccine safety has been recognized by regulatory experts and scientists involved in vaccine development [3]. In addition, there is a concern that expertise in performing the histopathological assessment of virus neurovirulence is waning [3]. To address these issues, we developed a quantitative method providing an objective assessment of virus neurovirulence by accurate measurement of virus-induced neuroinflammation and neurodegeneration. To this end, the immunoreactivity for the pan-T cell marker CD3 and pan-B cell marker CD20 measured by specific image analysis algorithms was shown to provide an excellent overall quantitative estimate of the lymphocytic infiltration [22]. In this study, the comparison of lymphocytic immunoreactivity in the CNS measured by AIA and inflammatory cell infiltration scores generated by histopathological analysis demonstrated strong and significant correlation between these two methods. However, the AIA provided a more accurate measure of lymphocytic infiltration since the issue of enumeration of perivascular cuffs which are varying in sizes and “thickness” [10,20], as well as possibility of overlooking diffuse parenchymal infiltration, is virtually eliminated as every immunostained lymphocyte in the CNS ROI is identified and analyzed independently of its location.

Our previous and current study demonstrated that AIA of the CD68-IR in virus-infected CNS provides a versatile and valuable tool for quantitative evaluation of the overall microglial activation including both focal and diffuse patterns (generally referred to as microgliosis). It should be emphasized that the diffuse patterns of microglial activation are difficult or impossible to measure using routine histological stains and conventional semi-quantitative scoring analysis. Therefore, the overall microglial activation induced by neurotropic viruses could be largely underestimated, yielding inconsistent and unreliable data. In addition, our observations suggest that the magnitude and extent of CD68-IR may serve as a reliable indirect marker of neurodegeneration because of the strong and significant negative correlation between microglial activation and neurodegeneration.

Finally, we describe the first use of image analysis for direct quantitative assessment of neurodegeneration induced by flaviviruses in the CNS of monkeys. One significant problem associated with the traditional semi-quantitative assessment of neurodegeneration in the virus-infected CNS is that the majority of grading scales include the percentage of neurons that were “changed or lost”. Given the enormous number of neurons in the affected regions of the primate CNS and considering the fact that unbiased stereological methods [25] were not used to assess the neuronal loss, it seems unlikely that such analysis provides a reliable evaluation of viral neurovirulence, and thus may fail to predict the safety of live virus vaccines. In contrast, our results show that quantitative analysis of immunoreactivity for neuron-specific antigen NeuN, a selective neuronal marker [26–30], is a useful and reliable method for the assessment of neurodegeneration in the virus-infected CNS. NeuN-immunostaining is remarkably superior to routine histological stains such as Nissl because it provides selective staining of neuronal nuclei, cytoplasm, and proximal processes with

greater intensity and better definition, and has the advantage of clear delineation of neurons from other cell types (personal observation and Refs. [28,29]). In this study, AIA revealed significant decrease of NeuN-IR in sites of neurodegeneration attributed to infection with more neurovirulent viruses (i.e., TBEV/DEN4Δ30 or LGTV). The decreased expression of neuronal protein NeuN was indicative of both neurodegeneration and neuronal loss. Although strong and significant correlations between NeuN-IR and relevant semi-quantitative scores were established in this study, we strongly believe that the quantitative analysis of neurodegeneration using neuronal markers provides a more reliable tool for evaluation of virus neurovirulence than the semi-quantitative analysis of routine stains, especially since the predominant cells infected by neurotropic viruses are neurons.

The quantitative approach described here measures the amount of immunoreactivity (number of positive pixels per mm^2 of tissue), and it is different from two-dimensional cell profile counting or stereological counting techniques. We believe that neither cell profile counting nor stereology could be reliably applied in the context of complex features of virus-induced neuroinflammation when individual inflammatory cells form densely packed layers or clusters. For assessment of virus neurovirulence, it is not important to know the absolute number of inflammatory cells or exact percentage of neurons that were lost. Rather, the meaningful quantitative comparisons can be made based on the magnitude of the cellular inflammatory responses and degree of virus-induced neurodegeneration measured by the amount of immunoreactivity for the relevant cellular marker using AIA.

In conclusion, we observed strong and significant correlations between quantitative measures of virus-induced neuroinflammation and neurodegeneration obtained by AIA and relevant semi-quantitative scores generated by conventional histopathological analysis suggesting that the outcomes of these two methods can be viewed as functions of one another. However, the presence of a correlation does not imply that these methods possess equal sensitivity and reproducibility. We show that AIA offers a number of significant advantages over traditional semi-quantitative approach. First, neuroinflammation and neurodegeneration are measured using specific cellular markers, thus providing in-depth information regarding the cell types involved in host response to viral infection of the CNS. Second, quantitative analysis of the immunoreactivity for each specific cell type provides an objective and accurate measure of the cellular inflammatory infiltration, microglial activation, and neurodegeneration regardless of their topographical patterns, thus eliminating the need for excessive manual counting and visual impression-based assessment. Third, the use of the AIA algorithms, once established, is relatively simple and time efficient. This is in contrast to semi-quantitative histopathological scoring, which is tedious and time-consuming. AIA algorithms can be applied to entire sections of the CNS regions, which dramatically reduces analysis time. Indeed, the time needed to apply the AIA algorithms within a given CNS region does not depend on the severity of neuroinflammation or neurodegeneration, while the time required for distinguishing, counting, and grading inflammatory lesions using a semi-quantitative approach is dependent on their severity. Fourth, this approach may be generally applicable for rapid and unbiased assessment of a wide variety of CNS pathologies. Because the AIA of neuroinflammation and neurodegeneration is an accurate and reliable method, it may enable robust statistical comparisons of viruses with varying neurovirulence, and may help to establish consistent analytical standards across laboratories and regulatory agencies. Given that an adequate number of cellular markers is analyzed, this method provides objective quantitative criteria for evaluation of virus neurovirulence and will facilitate decision-making regarding the safety of live virus vaccine candidates and their advancement to clinical evaluation in humans.

The feasibility of the AIA for studies of viral neuropathogenesis/neurovirulence and vaccine safety evaluation will rely on the accessibility of digital scanners and image analysis software to the scientific and regulatory communities. Nevertheless, once acquired, the digitalized whole-tissue section slides (virtual slides) can be stored indefinitely without loss of quality, and viewed, shared, annotated, and analyzed by multiple investigators in real time across the world. It is our hope that these outstanding advantages of modern digital pathology will markedly advance many fields of research including but not limited to virology, neuroinflammation, neuroscience, and vaccinology in the near future.

Supplementary Material

Refer to Web version on PubMed Central for supplementary material.

Acknowledgments

We acknowledge the staff of Bioqual, Inc. (Rockville, MD) and Pathology Associates Division of Charles River Laboratories (Frederick, MD), and Dr. J. Ward, Dr. R. Montali, Lawrence Faucette, Marina Rahman, and Katherine Shea (Comparative Medicine Branch, NIAID, NIH) for their help in conducting the studies. We also thank Drs. J. Taubenberger and S. Whitehead, NIAID, NIH for helpful discussions and critical reading of the manuscript. This work was supported by funds provided by the NIAID Intramural Research Program.

References

1. Afzal MA, Marsden SA, Hull RM, Pipkin PA, Bentley ML, Minor PD. Evaluation of the neurovirulence test for mumps vaccines. Biologicals. 1999; 27:43–9. [PubMed: 10441402]
2. Rubin SA, Snoy PJ, Wright KE, Brown EG, Reeve P, Beeler JA, et al. The mumps virus neurovirulence safety test in Rhesus monkeys: a comparison of mumps virus strains. J Infect Dis. 1999; 180:521–5. [PubMed: 10395874]
3. WHO. Final report. IABS Scientific Workshop on Neurovirulence Tests for Live Virus Vaccines. Geneva, Switzerland: WHO; 2005. p. 1-7.
4. Johnson JE, Nasar F, Coleman JW, Price RE, Javadian A, Draper K, et al. Neurovirulence properties of recombinant vesicular stomatitis virus vectors in non-human primates. Virology. 2007; 360:36–49. [PubMed: 17098273]
5. Levenbook I, Draper K. Neuropathogenesis and neurovirulence of live flaviviral vaccines in monkeys. J Virol. 2009; 83:5289–90. [PubMed: 19383635]
6. Maximova OA, Whitehead SS, Murphy BR, Pletnev AG. Neuropathogenesis and neurovirulence of live flaviviral vaccines in monkeys reply. J Virol. 2009; 83:5290–2.
7. Nathanson N, Goldblatt D, Thind IS, Davis M, Price WH. Histological studies of the monkey neurovirulence of group B arboviruses. I. A semi-quantitative grading scale. Am J Epidemiol. 1965; 82:359–81. [PubMed: 4285344]
8. Nathanson N, Davis M, Thind IS, Price WH. Histological studies of the monkey neurovirulence of group B arboviruses. II. Selection of indicator centers. Am J Epidemiol. 1966; 84:524–40. [PubMed: 4289010]
9. Nathanson N, Gittelsohn AM, Thind IS, Price WH. Histological studies of the monkey neurovirulence of group B arboviruses. III. Relative virulence of selected viruses. Am J Epidemiol. 1967; 85:503–17. [PubMed: 4290525]
10. Angsubhakorn S, Moe JB, Latendresse JR, Ward GS, Ngamprochana M, Sahaphong S, et al. The neurovirulence of flaviviruses in crab-eating monkeys (Macaca fascicularis). Southeast Asian J Trop Med Public Health. 1986; 17:604–12. [PubMed: 3033834]
11. Levenbook IS, Pelleu LJ, Elisberg BL. The monkey safety test for neurovirulence of yellow fever vaccines: the utility of quantitative clinical evaluation and histological examination. J Biol Stand. 1987; 15:305–13. [PubMed: 3680299]
12. WHO. Requirements for yellow fever vaccine. WHO Tech Rep Ser. 1998; 872:38–40.
13. Monath TP, Soike K, Levenbook I, Zhang ZX, Arroyo J, Delagrave S, et al. Recombinant, chimaeric live, attenuated vaccine (ChimeriVax™) incorporating the envelope genes of Japanese

encephalitis (SA14-14-2) virus and the capsid and nonstructural genes of yellow fever (17D) virus is safe, immunogenic and protective in non-human primates. Vaccine. 1999; 17:1869–82. [PubMed: 10217584]

14. Monath TP, Levenbook I, Soike K, Zhang ZX, Ratterree M, Draper K, et al. Chimeric yellow fever virus 17D-Japanese encephalitis virus vaccine: dose response effectiveness and extended safety testing in rhesus monkeys. J Virol. 2000; 74:1742–51. [PubMed: 10644345]
15. Monath TP, Arroyo J, Levenbook I, Zhang ZX, Catalan J, Draper K, et al. Single mutation in the flavivirus envelope protein hinge region increases neurovirulence for mice and monkeys but decreases viscerotropism for monkeys: relevance to development and safety testing of live, attenuated vaccines. J Virol. 2002; 76:1932–43. [PubMed: 11799188]
16. Marchevsky RS, Freire MS, Coutinho ES, Galler R. Neurovirulence of yellow fever 17DD vaccine virus to rhesus monkeys. Virology. 2003; 316:55–63. [PubMed: 14599790]
17. Guirakhoo F, Pugachev K, Zhang Z, Myers G, Levenbook I, Draper K, et al. Safety and efficacy of chimeric yellow fever-dengue virus tetravalent vaccine formulations in nonhuman primates. J Virol. 2004; 78:4761–75. [PubMed: 15078958]
18. Karganova GG, Pripuzova NS, Tereshkina NV, Gmyl' LV, Dzhivanian TI, Rumiantsev AA, et al. Residual neurovirulence of the chimera of Langat and Denge-4 flaviviruses in intracerebral infection of monkeys. Vopr Virusol. 2005; 50:27–31. [PubMed: 15747868]
19. Maximova OA, Ward JM, Asher DM, St Claire M, Finneyfrock BW, Speicher JM, et al. Comparative neuropathogenesis and neurovirulence of attenuated flaviviruses in nonhuman primates. J Virol. 2008; 82:5255–68. [PubMed: 18353947]
20. Fine DL, Roberts BA, Terpening SJ, Mott J, Vasconcelos D, House RV. Neurovirulence evaluation of Venezuelan equine encephalitis (VEE) vaccine candidate V3526 in nonhuman primates. Vaccine. 2008; 26:3497–506. [PubMed: 18508163]
21. Pripuzova NS, Tereshkina NV, Gmyl LV, Dzhivanyan TI, Rumyantsev AA, Romanova LIu, et al. Safety evaluation of chimeric Langat/Dengue 4 flavivirus, a live vaccine candidate against tick-borne encephalitis. J Med Virol. 2009; 81:1777–85. [PubMed: 19697399]
22. Maximova OA, Faucette LJ, Ward JM, Murphy BR, Pletnev AG. Cellular inflammatory response to flaviviruses in the central nervous system of a primate host. J Histochem Cytochem. 2009; 57:973–89. [PubMed: 19581627]
23. Budka, H. Neuropathology—the diagnostic approach. Garcia, JH.; Budka, H.; McKeever, PE.; Sarnat, HB.; Sima, AAF., editors. St. Louis: Mosby; 1997. p. 353-91.
24. Steiner I, Budka H, Chaudhuri A, Koskiniemi M, Sainio K, Salonen O, et al. Viral encephalitis: a review of diagnostic methods and guidelines for management. Eur J Neurol. 2005; 12:331–43. [PubMed: 15804262]
25. West MJ, Slomianka L, Gundersen HJ. Unbiased stereological estimation of the total number of neurons in the subdivisions of the rat hippocampus using the optical fractionator. Anat Rec. 1991; 231:482–97. [PubMed: 1793176]
26. Mullen RJ, Buck CR, Smith AM. NeuN, a neuronal specific nuclear protein in vertebrates. Development. 1992; 116:201–11. [PubMed: 1483388]
27. Wolf HK, Buslei R, Schmidt-Kastner R, Schmidt-Kastner PK, Pietsch T, Wiestler OD, et al. NeuN: a useful neuronal marker for diagnostic histopathology. J Histochem Cytochem. 1996; 44:1167–71. [PubMed: 8813082]
28. Jongen-Rêlo AL, Feldon J. Specific neuronal protein: a new tool for histological evaluation of excitotoxic lesions. Physiol Behav. 2002; 76:449–56. [PubMed: 12126979]
29. Gittins R, Harrison PJ. Neuronal density, size and shape in the human anterior cingulate cortex: a comparison of Nissl and NeuN staining. Brain Res Bull. 2004; 63:155–60. [PubMed: 15130705]
30. Lind D, Franken S, Kappler J, Jankowski J, Schilling K. Characterization of the neuronal marker NeuN as a multiply phosphorylated antigen with discrete subcellular localization. J Neurosci Res. 2005; 79:295–302. [PubMed: 15605376]
31. Pletnev AG, Men R. Attenuation of the Langat tick-borne flavivirus by chimerization with mosquito-borne flavivirus dengue type 4. Proc Natl Acad Sci USA. 1998; 95:1746–51. [PubMed: 9465088]

32. Rumyantsev AA, Chanock RM, Murphy BR, Pletnev AG. Comparison of live and inactivated tick-borne encephalitis virus vaccines for safety, immunogenicity and efficacy in rhesus monkeys. Vaccine. 2006; 24:133–43. [PubMed: 16115704]

33. Martin, RF.; Bowden, DM. Primate brain maps: structure of the macaque brain. Amsterdam: University of Washington, Elsevier; 2000.

Appendix A. Supplementary data

Supplementary data associated with this article can be found, in the online version, at doi: 10.1016/j.vaccine.2010.07.070.

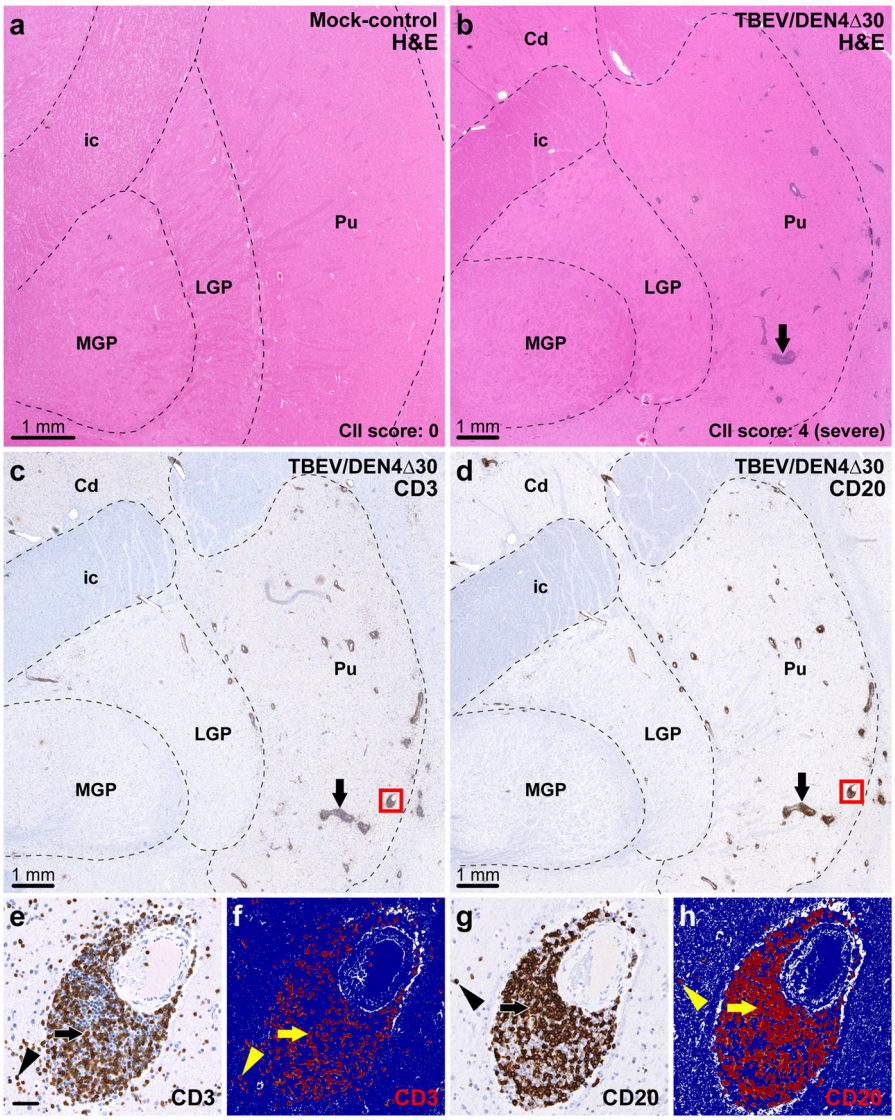

Fig. 1.

Assessment of lymphocytic infiltration in the basal ganglia. (a) Representative section through the basal ganglia of a mock-inoculated monkey (H&E staining). (b–d) Adjacent sections through the basal ganglia of a TBEV/DEN4Δ30-infected monkey (CII score: 4, severe). The dashed lines in (a–d) show approximate boundaries of the basal ganglia visible in the sections. (b) H&E staining showing perivascular inflammatory infiltrates. (c) Infiltration by T cells as revealed by CD3-immunostaining. (d) Infiltration by B cells as revealed by CD20-immunostaining. Arrows in (b–d): large perivascular inflammatory infiltrates. (e–h) Original and corresponding markup images of the same blood vessel and surrounding parenchyma (red boxes in c and d) are shown at higher magnification. The results of applied CD3-IR or CD20-IR algorithms are shown in the markup images (f and h, respectively) where the positive pixels appear in red, negative pixels appear in dark blue, and neutral pixels (neither positive nor negative) appear in white. (e and f) CD3-immunoreactivity within the perivascular space (arrows) and parenchyma (arrowheads). (g and h) CD20-immunoreactivity within the perivascular space (arrows) and parenchyma

(arrowheads). *Abbreviations*: Cd, caudate nucleus; ic, internal capsule; MGP, medial globus pallidus; LGP, lateral globus pallidus; Pu, putamen. Bar in (e) (50 μm) also applies to (f–h).

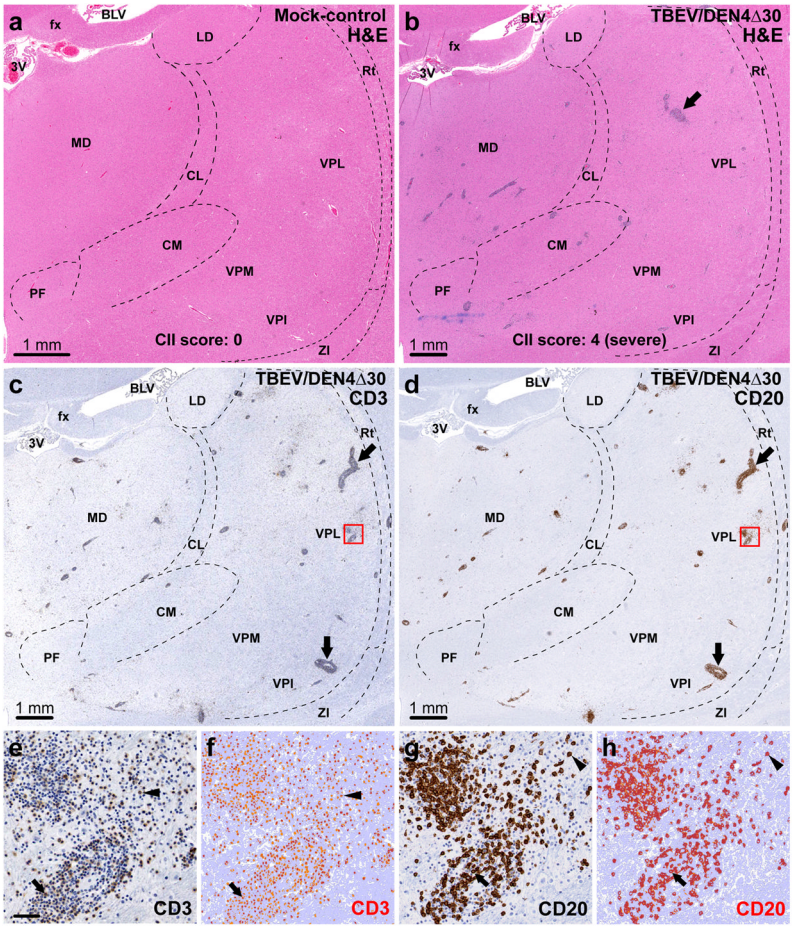

Fig. 2.

Assessment of lymphocytic infiltration in the thalamus. (a) Representative section through the thalamus of a mock-inoculated monkey (H&E staining). (b–d) Adjacent sections through the thalamus of a TBEV/DEN4Δ30-infected monkey (CII score: 4, severe). The dashed lines in (a–d) show approximate boundaries of the thalamic nuclei present in the sections. (b) H&E staining showing perivascular inflammatory infiltrates. (c) Infiltration by T cells (CD3-immunostaining). (d) Infiltration by B cells (CD20-immunostaining). Arrows in (b–d): large perivascular inflammatory infiltrates. (e–h) Original and corresponding markup images of the boxed areas in (c and d) are shown at higher magnification. The results of applied CD3 or CD20-IR algorithms are shown in the markup images (f and h, respectively) where the positive pixels appear in orange-red, negative pixels appear in light blue, and neutral pixels appear in white. (e and f) CD3-IR within the perivascular inflammatory infiltrate (arrows) and parenchyma (arrowheads). (g and h) CD20-IR within the perivascular inflammatory infiltrate (arrows) and parenchyma (arrowheads). *Abbreviations*: 3V, third ventricle; fx, fornix; BLV, body of lateral ventricle; LD, lateral dorsal nucleus; MD, medial dorsal nucleus; CL, central lateral nucleus; VPL, ventral posterolateral nucleus; Rt, reticular nucleus; PF, parafascicular nucleus; CM, centromedian nucleus; VPM, ventral posteromedial nucleus; VPI, ventral posteroinferior nucleus; ZI, zona incerta. Bar in (e) (50 μm) also applies to f–h.

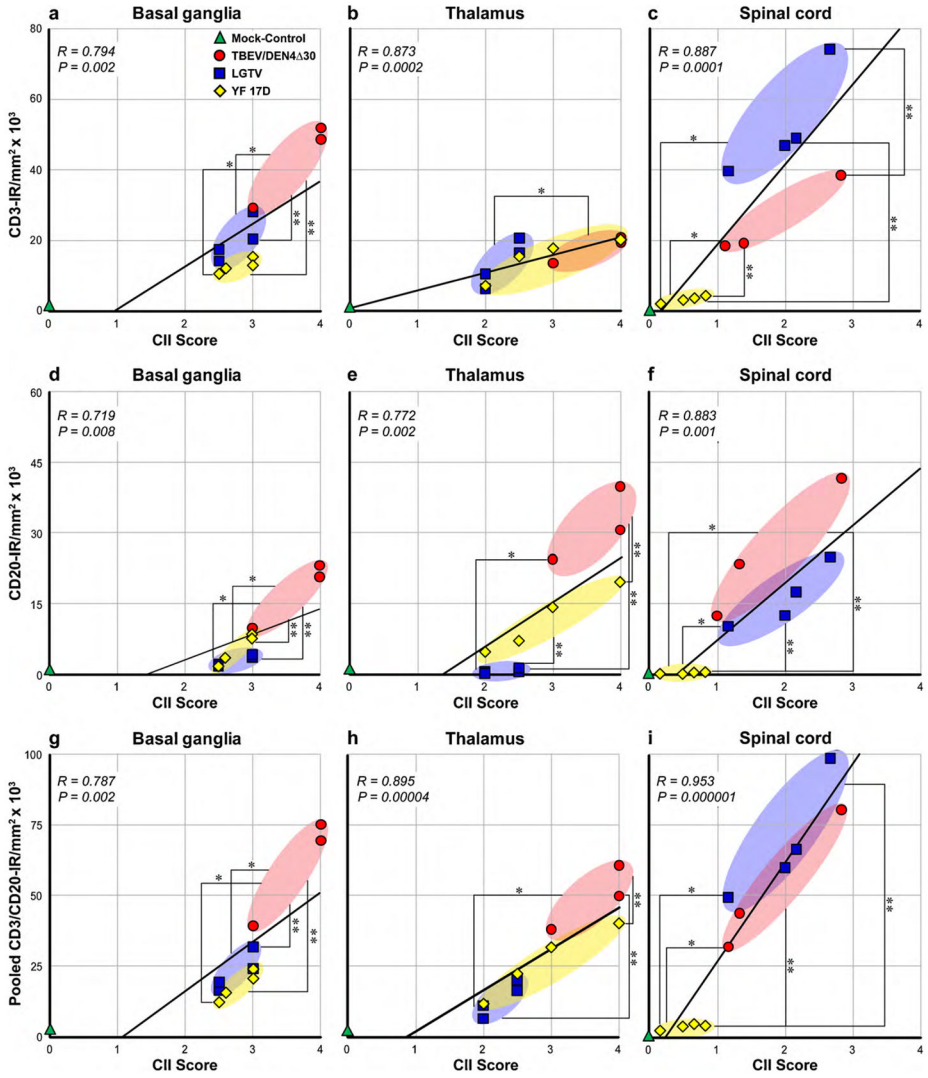

Fig. 3.

Analysis of correlation between CD3-IR, CD20-IR, or pooled CD3/CD20-IR and histopathological scores for cellular inflammatory infiltration (CII) in the CNS. Correlation between CD3-IR (a–c), CD20-IR (d–f), or pooled CD3/CD20-IR (g–i) and CII scores in the basal ganglia, thalamus, and spinal cord of mock-control monkey (green; $n = 1$) and monkeys infected with TBEV/DEN4Δ30 (red; $n = 3$), LGTV (blue; $n = 4$), or YF 17D (yellow; $n = 4$). The trend line, correlation coefficient (R), and P-value are shown in each plot. CII scores and IR values did not differ statistically between the viruses unless specifically noted. The statistically significant differences between the viruses based on mean CII scores are indicated with one asterisk and based on mean IR values are indicated with two asterisks ($P < 0.05$).

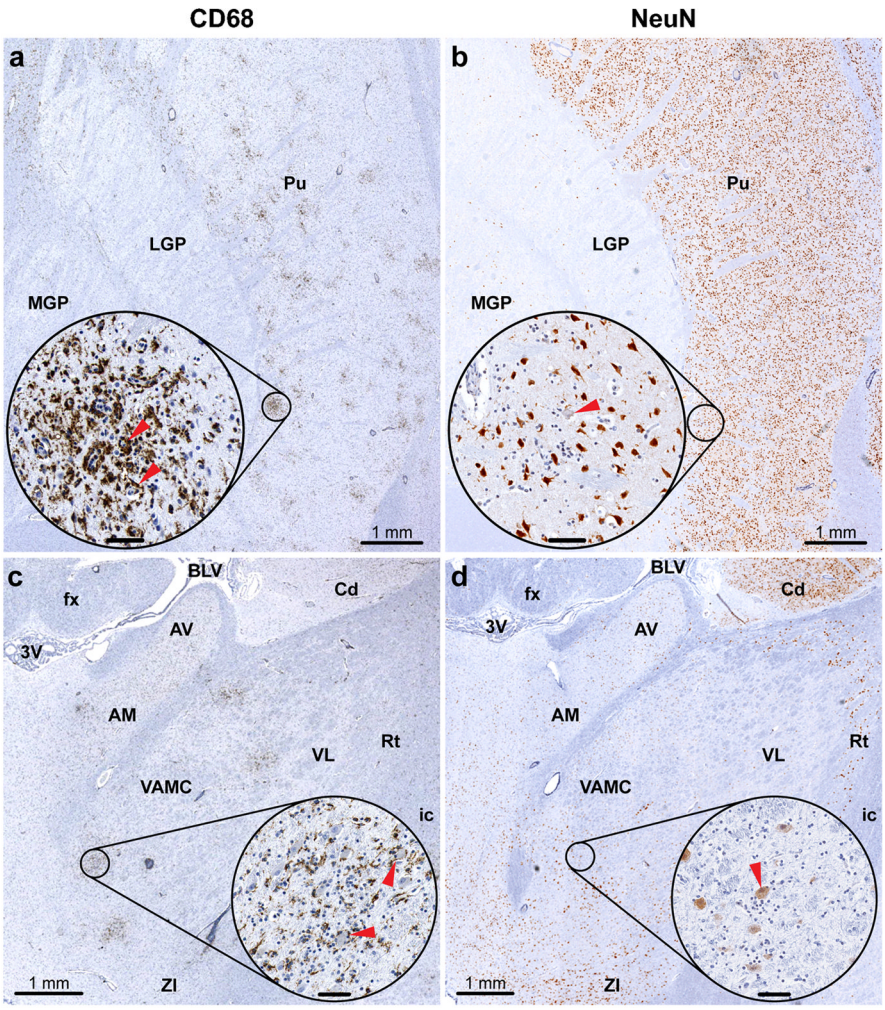

Fig. 4.

Assessment of microglial activation and neuronal degeneration in the basal ganglia and thalamus. Adjacent sections through the basal ganglia (a and b) and thalamus (c and d) of a YF 17D-infected monkey showing immunostaining for CD68 (a and c) or NeuN (b and d). The circled areas in (a–d) are shown at higher magnification in corresponding insets. Insets in (a and c) show CD68-immunoreactive activated microglia engulfing or in close contact with degenerating neurons (red arrowheads). Insets in (b and d) show degenerating neurons with eccentric nuclei and/or shrunken cytoplasm and decreased intensity of the NeuN signal (red arrowheads). *Abbreviations*: MGP, medial globus pallidus; LGP, lateral globus pallidus; Pu, putamen; 3V, third ventricle; fx, fornix; BLV, body of lateral ventricle; Cd, caudate nucleus; AV, anteroventral nucleus; AM, anteromedial nucleus; VL, ventral lateral nucleus; VAMC, magnocellular part of ventral anterior nucleus; Rt, reticular nucleus; ic, internal capsule; ZI, zona incerta. Inset bars: 50 μm.

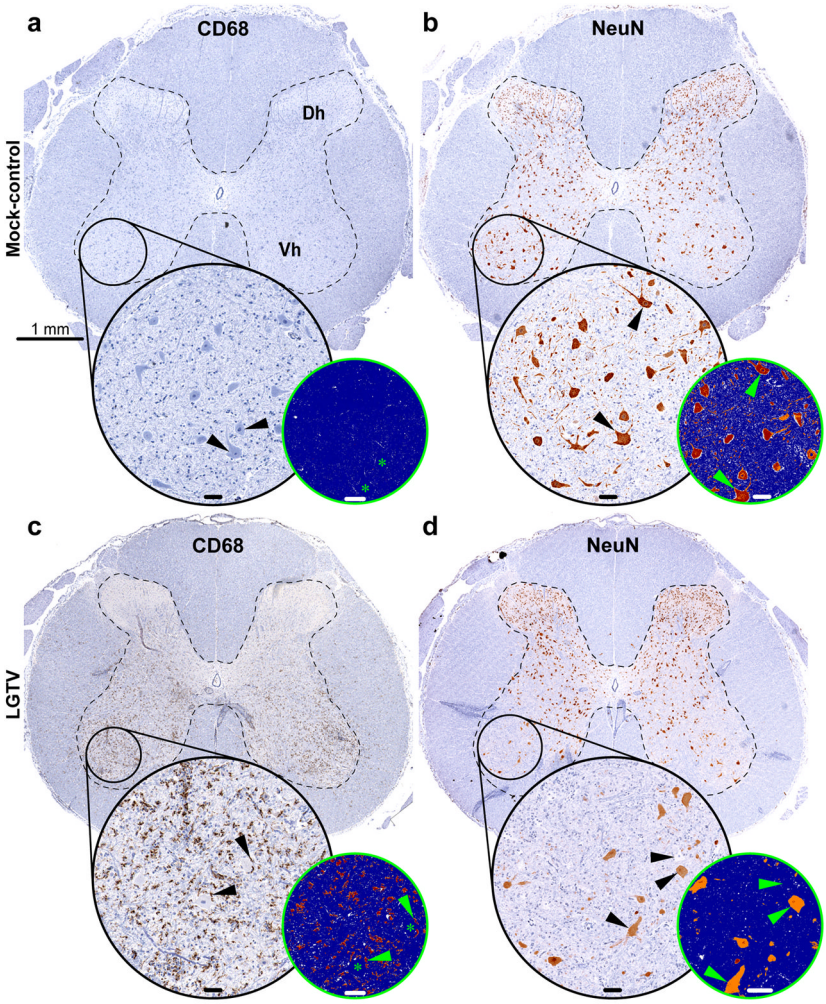

Fig. 5.

Image analysis of microglial activation (CD68-IR) and neurodegeneration (NeuN-IR) in the spinal cord. Adjacent transverse sections of the lumbar spinal cord of a mock-inoculated monkey (a and b) or LGTV-infected monkey (c and d) showing the analysis of CD68-IR (a and c) or NeuN-IR (b and d). The dashed lines show the approximate boundaries of the grey matter. The circled areas in (a–d) show the ventrolateral column containing motor neurons. The corresponding insets in (a–d) show the circled areas at higher magnification. Additional smaller insets in (a–d) represent markup images with applied CD68-IR or NeuN-IR algorithm (strong positive pixels, red; moderate positive pixels, orange; weak positive pixels, yellow; negative pixels, blue; neutral pixels, white). Note the CD68-IR surrounding degenerating neurons (black or green arrowheads in insets in c) and absence of CD68-IR in (a). Black arrowheads in (a) show normal motor neurons. Asterisks in (a and c) show the position of the corresponding neurons in the markup images. Note the strong NeuN-IR in the normal neurons (black or green arrowheads in b) and decreased number of neurons in (d). NeuN-IR in the remaining neurons is decreased or absent (black or green arrowheads in d). *Abbreviations*: Dh, dorsal horn; Vh, ventral horn. Bar in (a) also applies to (b–d); inset bars: 50 μm.

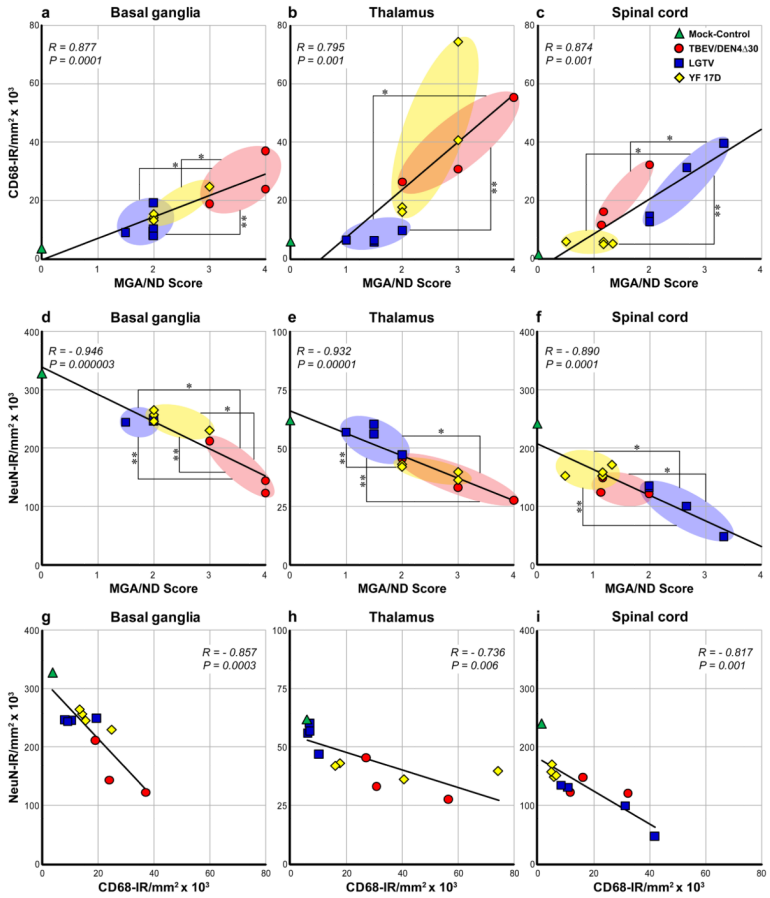

Fig. 6.

Analysis of correlation between CD68-IR and NeuN-IR and histopathological scores for microglial activation/neuronal degeneration (MGA/ND) in the CNS. Correlation between CD68-IR (a–c) or NeuN-IR (d–f) and MGA/ND scores in the basal ganglia, thalamus, and spinal cord of mock-inoculated control monkey (green; $n = 1$) and monkeys infected with TBEV/DEN4Δ30 (red; $n = 3$), LGTV (blue; $n = 4$), or YF 17D (yellow; $n = 4$). (g–i) Correlation between NeuN-IR and CD68-IR. The trend line, correlation coefficient (R), and P-value are shown in each plot. MGA/ND scores and IR values did not differ statistically between the viruses unless specifically noted. The statistically significant differences between the viruses based on mean MGA/ND scores are indicated with one asterisk and based on mean CD68-IR or NeuN-IR are indicated with two asterisks ($P < 0.05$).